Fiber drawing ability and loss optimization of niobium rich borophosphate optical glass fibers

Georges El Dib, Ronan Lebullenger, Laura Loi, Thierry Pain, Frédéric Adamietz, Lionel Canioni, Thierry Cardinal, Sébastien Chenu, Sylvain Danto

Fiber drawing ability and loss optimization of niobium rich borophosphate optical glass fibers

Georges El Dib[1,2], Ronan Lebullenger[3], Laura Loi[4], Thierry Pain[3], Frédéric Adamietz[5], Lionel Canioni[4], Thierry Cardinal[1], Sebastien Chenu[2,3], Sylvain Danto[1*]

[1]*Institute of Chemistry of the Condensed Matter (ICMCB), University of Bordeaux, 33600 Pessac, France*

[2]*Institute of research for ceramics (IRCER), European Ceramics Center, University of Limoges, 87000 Limoges, France*

[3]*Rennes Institute of Chemical Sciences (ISCR), University of Rennes, 35042 Rennes, France*

[4]*Center for intense lasers and applications (Celia), University of Bordeaux, 33400 Talence, France*

[5]*Institute of molecular science (ISM), University of Bordeaux, 33400 Talence, France*

*contact: sylvain.danto@u-bordeaux.fr

Abstract

Here we explore the manufacturing of niobium-rich borophosphate glasses into fibers with optical quality. Glass preforms of composition [(100-*x*) (0.95 $NaPO_3$ + 0.05 $Na_2B_4O_7$) - *x* Nb_2O_5] with *x* = 37, 38, 39, 40 were synthetized and thermally drawn. Viscosity measurements performed in the softening point range show that the optical fiber drawing temperature gradually increases with the amount of niobium oxide. X-ray diffraction and Raman structural analysis performed post drawing demonstrate that the BPN glass with 39% Nb_2O_5 represents the upper limit for fiber drawing under oxygen. Subsequently, preform quenching protocol was optimized to mitigate the density fluctuations within the glass matrix related to convection flows and compare with the conventional cast-in-mold method. Optical transmission and shadowscopy imaging highlight the improvement in the optical quality of the glasses produced following this new protocol. This observation is confirmed by cut back loss measurements which show a decreasing in the attenuation from 6.04 dB/m to 3.19 dB/m between the two methods. One believes the manufacturing of niobium rich borophosphate fibers with improved optical quality highlights their potential to be used as near-infrared highly nonlinear waveguide devices.

Keywords : Niobium rich glasses, drawing ability, density fluctuations, shadowscopy, optical fibers, loss optimization

1 Introduction

Niobium borophosphate glasses ($NaPO_3$ - $Na_2B_4O_7$ - Nb_2O_5) with high niobium oxide concentration (11 to 43 molar %) possess both excellent linear and nonlinear optical properties [1-3]. They offer a wide optical transparency range, extending from ~400 nm up to 2.5 µm. Numerous studies have focused on structural properties as well as the relation between the composition and the linear and non-linear effects of these glasses. They have reported a strong Kerr effect response in these glasses [1], obtaining thus a high second order susceptibility in the glass after thermal poling [4, 5]. The potential use of these glass materials is directly related to their ability to be shaped and integrated into optical devices. For instance, Karam *et al.* [6] prepared rich sodo-niobate thin films, reporting thus the highest second order nonlinear response recorded to date in an inorganic material ($\chi^{(2)}$=29 pm.V^{-1} at 1.06 µm). Optical fibers represent another important class of devices for optic and photonics applications. Hence, here we investigate more extensively the ability of materials in the $NaPO_3$ - $Na_2B_4O_7$ - Nb_2O_5 system to be

drawn into fibers of optical quality. To the best of our knowledge, one study only reports on an attempt to draw Er^{3+} doped niobium borophosphate glass containing 40 mol% of niobium oxide [7].

Firstly, preforms with increasing amount of Nb_2O_5 concentrations (37, 38, 39, 40 molar %) were synthesized and drawn to determine the concentration limit of niobium oxides enabling the fabrication of optical fibers, while still maintaining a high nonlinearity needed for further applications. Thermal, structural, rheological and optical properties of the glasses are presented. Secondly, the relationship between glass processing and optical loss in order to guarantee the potential use of niobium borophosphate glasses as fiber optic waveguides is investigated. Losses are originated from extrinsic chemical impurities including hydrogen or metallic impurities [8], but also from scattering due to density fluctuations and thus to refractive index fluctuations in the glass [8, 9]. Together these unwanted defects subsequently behave as specific absorption bands, possible crystallite nucleating sites and scattering centers, which can interfere with light propagation through the material in the spectral region of interest.

Here the specific contribution to optical loss due to scattering from density fluctuations was analyzed and discussed for various quenching protocols of the preform. There are three main measuring techniques to analyze glass material inhomogeneity, namely the classical Topler Schlieren darkfield method [10]. An additional possibility is the interferometric characterization. A third method is the production of a shadow image through the glass sample [11, 12]. In This work, we use the shadowscopy technique to extract information about the overall homogeneity of the prepared glass samples. Shadowscopy imaging reveals a large reduction in the magnitude of density fluctuations within the glass preform subjected to adjusted preparation method. This result is corroborated by cut-back measurements which shows a significant decrease in the loss of the resulting fiber.

2 Experimental

2.1 Glass synthesis and preform elaboration

Niobium borophosphate glasses (BPNx) of composition (100-*x*) (0.95 $NaPO_3$ + 0.05 $Na_2B_4O_7$) - *x* Nb_2O_5 were synthetized with *x* = 37, 38, 39, 40 the molar percentage of niobium oxide. High purity raw material powders, $NaPO_3$ (Alfa Aesar > 98%), $Na_2B_4O_7$ (Alfa Aesar 99.5%) and Nb_2O_5 (Alfa Aesar 99.9985%) were mixed in stoichiometric ratios. The mixture is then heated up in a platinum crucible at 1250 °C for 2 hours while stirring equally all the samples.

Two synthesis protocols detailed hereafter were explored to show how temperature gradients and convection flows impact glass density fluctuations and resulting fiber loss. In first case, casted preforms (later referred to as $(BPNx)_C$ for "Casted") were synthetized using the conventional direct quenching of the melt in a mold. The method involves the pouring of the heated up liquid into a stainless steel cylindrical mold preheated at 20 °C below T_g, then annealed for 10 hours before being slowly cooled down (~ 3 °C/min) to room temperature to remove residual mechanical stress. The resulting glass rods (10 mm of diameter and 8 cm long length) were then used for testing the fiber drawing ability. Unlike casting, the uncasting method consists in maintaining the glass in the crucible all along the quenching step. The uncasted preforms are referred to as $(BPNx)_{UC\text{-}T°C}$ for "Uncasted" with *T* being the temperature at which the crucible is removed from the furnace. After the melting step at 1250 °C, the glass is cooled down (~20 °C/min) in the furnace until 1150 °C or 1100 °C, then let to cool down until room temperature in open air. The glass is then removed from the crucible and annealed for 10 hours at T_g - 20 °C before being mechanically drilled into a cylindrical preform (8 mm of diameter and 4 cm long length).

Inductively conducted plasma-optical emission spectrometry (ICP/ES) was conducted with a Thermo Fisher Varian ICP/OES 720 ES apparatus.

2.2 Physico-chemical and thermal characterizations

Density measurements of the glasses were performed using the Archimedes principle by immersing the samples in Diethyl-phthalate, which the density as a function of temperature is well known, with an estimated error of 0.02 g/cm^3.

The glass transition temperatures (T_g) and the onset of crystallization temperatures (T_x) were determined using differential thermal analyses (DTA) on a TA instruments Model SDT 2960 with a precision of ±2 °C and a 10°C/min heating rate. 50 mg of bulk glass samples were placed in a platinum crucible while a second empty platinum crucible was used as a reference sample. The T_g and T_x temperatures were determined as the onset of the thermal phenomena from the tangent intersection of the DTA curves. The crystallization temperature while cooling the melt of BPN39 is identified by DTA with a cooling rate of 20 °C/min from 1250 °C.

Viscosity measurements were performed on cylindrical samples of 4 mm length and 7.7 mm diameter using a parallel-plate viscometer (Theta) from room temperature up to T_{max} at a heating rate of 5 °C/min. T_{max} being determined by the minimal sample thickness required for a measurement between the plates, which is 1.1 mm. A load of 200 g was applied to induce deformation of the glass. Viscosity was determined in the region of [$10^{8.5}$ – $10^{4.75}$] Pa.s.

2.3 Structural characterizations

The amorphous state of the samples was confirmed with X-ray powder diffraction (XRD). XRD patterns were collected on Philips Xpert powder diffractometer (CuK_α-radiation, theta-theta geometry, reflection mode) at room temperature and (8-80) angular range. The counting step and time were 0.0167° and 5.66 seconds respectively. Crystalline phases were identified using the EVA software.

Raman spectra were recorded with a LabRAM confocal micro-Raman instrument (typical resolution of 3 cm^{-1}), in the backscattering geometry at room temperature. The 532nm continuous laser was used for excitation.

2.4 Fiber drawing

The optical fibers were drawn using a 3 meters high optical fiber drawing tower with an electrical furnace with a sharp temperature profile. First, the preform is heated up to its softening temperature at 15 °C/min to initiate the elongation process. Once the drop is formed and tied on the drum the preform is slowly fed into the furnace while the drawing parameters (temperature, drum speed, feed rate) are continuously monitored. Preforms were successfully drawn into tens of meters long fibers with diameters ranging from 150 µm to 250 µm. The process was performed under an oxygen gas flow (2 L/min) to avoid any external pollution of the glass surface and to prevent the Nb^{5+} reduction into Nb^{4+}.

2.5 Optical characterizations

The linear refractive indices were measured on the bulk samples using the Brewster's angle method at 935 nm.

Optical transmission spectra (UV-Visible-NIR) in the wavelength range 300-2500 nm were measured with a double-beam spectrophotometer (Cary 5000 Varian) at room temperature. Optically polished samples with ~1.2 mm thickness were used for the measurements.

Visualization of inhomogeneities in the bulk glasses prior to fiber drawing was performed by shadowscopy, which consists in analyzing on a screen the projected shadow of an illuminated sample. A He-Ne 632.8 nm laser source is focalized with a mitutoyo objective (20x, NA 0.42) on a sample polished on both sides. The laser, the objective, the sample and the diffusion screen are aligned on the

same optical axis. Images were taken with a high resolution camera ''Sony A7 III''. The sample rests on a ''xyz'' micropositioner which allows any region of the sample to be placed in the beam. The sample can be rotated (±10°) to eliminate surface flaws.

Attenuation measurement in optical fibers was recorded using the well-established cut back method. Both ends of the fiber were manually cleaved with a diamond blade and quality of the cleaving was inspected after each cut with an optical microscope. A 1 µm laser source was coupled into the fiber. At the other end of the fiber, the transmitted light was collected using Thorlabs optical power meter (S121C).

3 Results and discussion

3.1 Materials properties and fiber drawing ability

Here, we investigate the ability of BPN oxide glasses to be drawn from the preform into fibers with high nonlinearity and improved optical properties. The investigated glass materials (acronyms, nominal compositions in molar and cationic percent, cationic % measured by ICP) are summarized in Table 1. In previous work, Cardinal *et al.* [1] report that the $\chi^{(3)}$ of BPN glasses (x = 0 to 43 mol%) increases with niobium oxide concentrations while their thermal stability decreases in the meantime. The glass compositions selected here result from a trade-off between these two criteria. The (BPNx) glasses with x = 37 to 40 mol% exhibit the highest nonlinear response while maintaining the required thermal stability to be drawn into optical fibers.

Table 1. Nominal compositions (mol and cationic %) and measured elemental composition (cationic %) by ICP of the fiber preforms

	Nominal compositions (mol %)			Nominal compositions (Cationic %)				Measured compositions (Cationic % ±0.5)			
Sample	$NaPO_3$	$Na_2B_4O_7$	Nb_2O_5	Na	P	B	Nb	Na	P	B	Nb
$(BPN37)_C$	59.8	3.2	37.0	31.1	28.2	5.9	34.8	30.8	28.7	5.5	35.0
$(BPN38)_C$	58.9	3.1	38.0	30.6	27.7	5.8	35.8	30.8	27.4	5.5	36.3
$(BPN39)_C$	58.0	3.0	39.0	30.2	27.3	5.7	36.8	30.3	27.9	5.2	36.6
$(BPN40)_C$	57.1	2.9	40.0	29.7	26.9	5.6	37.8	30.1	26.7	5.4	37.8

The comparison between the nominal and measured compositions for each preform are found to be similar within the measurement accuracy. In Table 2 are given the physicochemical properties of the investigated glasses: T_g, T_x and the difference $\Delta T = T_x - T_g$, as well as the density and the linear refractive index at 935 nm.

Table 2. Physicochemical properties of the investigated glasses : glass transition (T_g) and onset of crystallization (T_x) temperatures, thermal stability against crystallization (ΔT), glass density (ρ) and refractive index at 532 nm.

Sample	T_g (± 2°C)	T_x (± 2°C)	ΔT (± 4°C)	ρ (±0.02g/cm^3)	$n_{935\ nm}$ (±0.005)

$(BPN37)_C$	602	818	216	3.48	1.806
$(BPN38)_C$	608	806	198	3.51	1.808
$(BPN39)_C$	615	785	170	3.53	1.822
$(BPN40)_C$	620	780	160	3.55	1.841

With the Nb_2O_5 concentration increasing, T_g increases and T_x decreases progressively. In addition, the difference ΔT between the two characteristic temperatures T_g and T_x is most of the time regarded as a reliable criterion to evaluate the glass thermal stability *vs* crystallization, in particular for its shaping by thermal process like glass fiber drawing, with targeted values of $\Delta T \geq$ 100-120 °C. Judging from the ΔT value, we observe a gradual destabilization towards devitrification for an increasing amount of transition ions introduced. Yet all compositions, regarding the ΔT criterion, appear compatible with fiber drawing. The density of the (BPNx) glasses ranges from ρ = 3.48 g.cm^{-3} up to 3.55 g.cm^{-3}, which is in good agreement with Cardinal *et al*. [3]. One can also note an increase of the refractive index with niobium oxide content from 1.806 to 1.841, an evolution due to the higher polarizability with the niobium content. An understanding of the glass viscosity behavior when close to its softening point (~$10^{5.5}$ Pa·s) is required for defining the appropriated temperature for fiber drawing processing. In Figure 1, the viscosity behavior of the $(BPNx)_C$ compositions measured by parallel-plate viscometer as a function of the temperature is depicted.

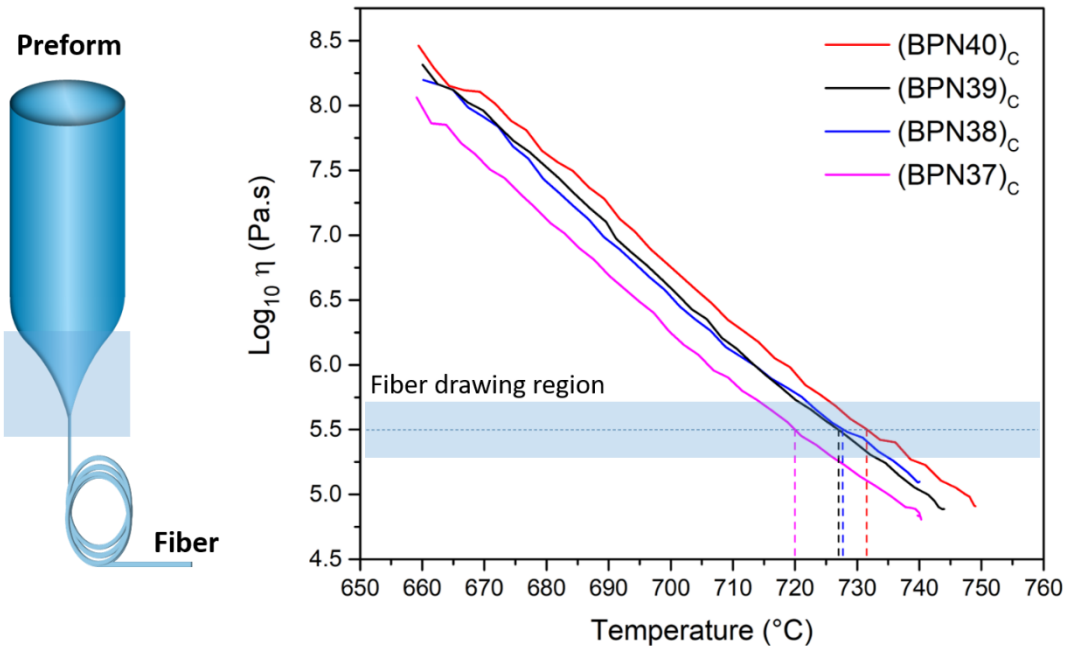

Fig 1. Scheme of the preform-to-fiber thermal drawing process (left) and viscosity behavior of the investigated glasses as a function of the temperature (right)

We notice a shift of the viscosity to the higher temperatures with the increase of niobium oxide content. At 720°C, we reach a viscosity of $10^{5.5}$ Pa.s for BPN37, while this value is reached at 732°C for BPN40. This is linked to the difference in *Tg* between BPN37 (T_g = 602 °C) and BPN40 (T_g = 620 °C), characteristic of chemical bonds with higher strength, requiring thus a higher temperature to be deformed. The glass network structure and viscosity range are in good agreement with a study

performed on a commercial glass from SCHOTT (P-SF67) containing niobium oxide [13]. Based on viscosity measurements, the drawing temperature was estimated to be ~720 °C to ~732 °C for the BPN37 to BPN40 respectively. Those assumptions were experimentally verified as the BPN37, BPN38 and BPN39 preforms could be continuously drawn in the 715-740 °C temperature range for several meters with diameters ranging 150-250 µm.

Drawing ability is directly related to the thermal stability against devitrification of a glass. The process consists in raising the temperature of the preform to the appropriated softening point without exceeding the onset of crystallization temperature (T_x) to avoid any form of crystallization. Structural analysis were performed on the BPN fibers after drawing to determine the niobium oxide upper limit compatible with fiber processing. XRD patterns of the fibers are depicted in Figure 2.a while a micrograph of the preform neck-down of BNP 39 and BPN40 is shown in inset.

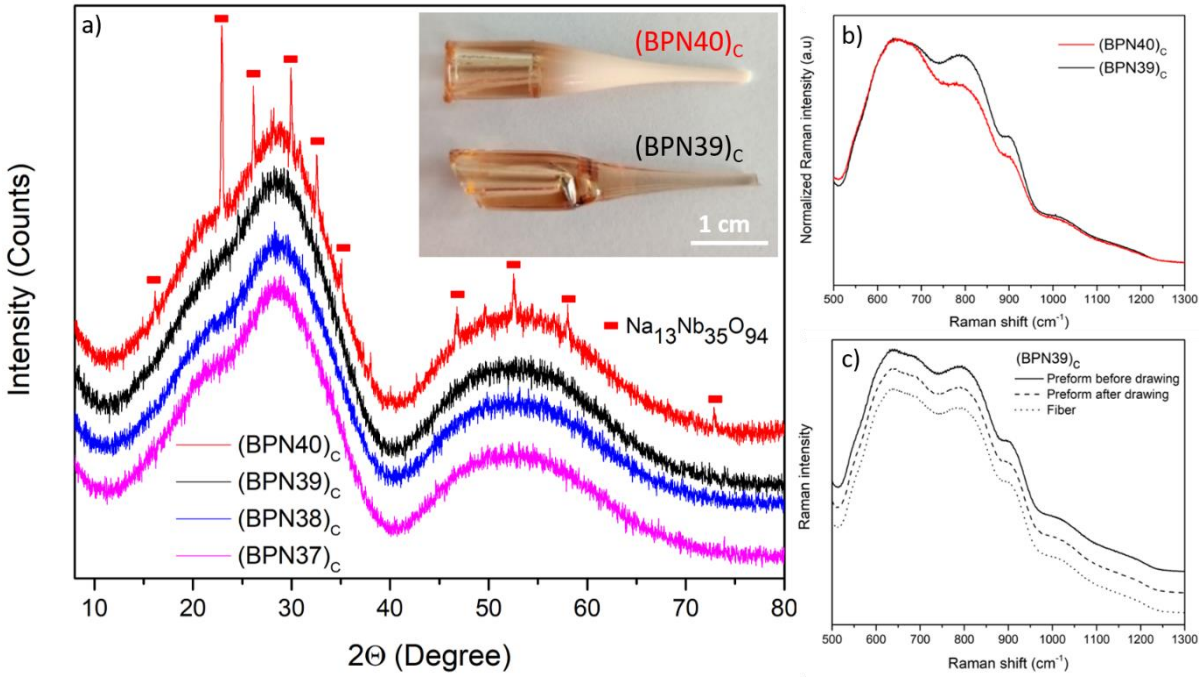

Fig 2. a) XRD pattern on BPN fibers after drawing and a photo of the preform neck-down of BNP39 and BPN40 is shown in inset. b) Raman spectrum on the neck down area, on both BPN39 and BPN40 and c) Raman spectrum of a BPN39, on the preform before the drawing process after the drawing process and on the fiber

XRD analyses of the BPN containing 39 mol% or below of niobium oxide show halos typical of an amorphous material. For 40% Nb_2O_5, XRD analysis presents mixed crystalline peaks best indexed by the isostructural phase $Na_{13}Nb_{35}O_{94}$ (ICSD N° 24882). This phase is similar to a $Na_{13}Nb_{35}O_{94}$ phase generated after thermal treatment of a BPN42 at 600°C for 6 hours [14]. In agreement with XRD patterns, while micrograph of the BPN39 preform neck-down shows no signs of heterogeneities or inclusions, the preform neck-down of the BPN40 show detrimental modification preventing the drawing of fibers of optical quality. It is worth noticing that all fiber drawing experiments of the (BPNx) glasses were conducted under controlled oxygen flux (3 $l.min^{-1}$). The atmosphere in the furnace also has a strong impact on the crystallization. Previous studies, conducted on fluoride and tellurite glasses, have demonstrated the ability to avoid crystallization during the fiber drawing process by controlling the atmosphere in the furnace [15, 16]. Considering borophosphates, Petit *et al.* [7] reported on the fiber drawing under helium of Er^{3+} doped BPN with 40 mol% of niobium oxide. Yet, due to helium, a

major reduction of niobium ions from Nb^{5+} to Nb^{4+} was observed. It led to a drastic loss in optical quality of the resulting fibers, making them unpractical for further applications.

Structural comparison between the BPN39 and BPN40 glasses after drawing were completed using Raman spectroscopy. Figure 2.b shows normalized Raman spectra (500-1300 cm^{-1}) on the neck-down area of the preforms for both glasses. It highlights the structural modification undergone by the BPN40 glass during fiber drawing due to its devitrification. Crystallization initiates the weakening of the bands at 810 and 905 cm^{-1} and intensifies the band centered at 640 cm^{-1}. Such modification of these bands intensities could be attributed to a progressive distortion of the niobate network [14, 17]. Similar comparison is performed on the BPN39 preform before and after drawing as well as on the fiber to pinpoint structural deviation induced by the drawing process (Figure 2.c). The three normalized Raman signatures precisely overlap meaning that no structural modification occurred during the drawing process of BPN39 glasses. The structure of the glass is well identified in previous works [3, 18]. Three bands can be clearly identified at 640, 810 and 905 cm^{-1}. The broad band at 640 cm^{-1}, is attributed to Nb–O modes with Nb–O–Nb, indicative of a three-dimensional niobium oxygen framework. The band at 810 cm^{-1} can be attributed to NbO_6 octahedra possessing both Nb–O–Nb and Nb–O–P or Nb–O–B connections to corner shared NbO_6 octahedra. The band at 905 cm^{-1} can be attributed to Nb–O short bonds from distorted NbO_6 octahedra connected to an alkali atom. Raman modes above 960 cm^{-1} are assigned to vibrational modes of P-O bonds. Evidence from X-ray diffraction and Raman structural analysis show that the BPN glass with 39 mol% of Nb_2O_5 represents the upper limit for fiber drawing under oxygen.

3.2 Loss optimization

The main objective in the current study is the manufacturing of BPN glass fibers of optical quality. The elaboration of the BPN preforms typically involves the direct pouring of the heated up mixture into a stainless steel cylindrical mold preheated at 20 °C below T_g which creates convection flows leading so to density fluctuations within the glass cylindrical preform. In order to estimate how this step affects density fluctuations within the glass, a series of bulk samples were prepared following an alternative strategy. In this case, after melting at 1250 °C, the glass was let to cool down in the furnace, then air cooled to room temperature while in the crucible. Only after completing cooling down and annealing, the glass was mechanically drilled into a preform (see *Experimental* for further details). The crystallization temperature while cooling the melt is identified by DTA with a sharp exothermic peak at 1020°C (Fig 1-SI). As a consequence, the removing of the melt from the furnace was performed at 1150°C and 1100°C to compare the respective optical quality of the samples.

Optical transmission of polished BPN39 bulk samples with similar thicknesses prepared following the different protocols are depicted on Figure 3.a. One notes a gradual improvement in the overall transmission of the glasses as well as in the band gap region between the casted, uncasted @1150 °C and uncasted @1100 °C samples respectively. The maximum transmission of the material, taking into account the Fresnel losses and the reflections on both face of the sample, was calculated to be 84% using the following equation: $T_{max} = \frac{2n}{n^2+1}$. Only the uncasted samples approach this maximum value, while the casted sample remains under.

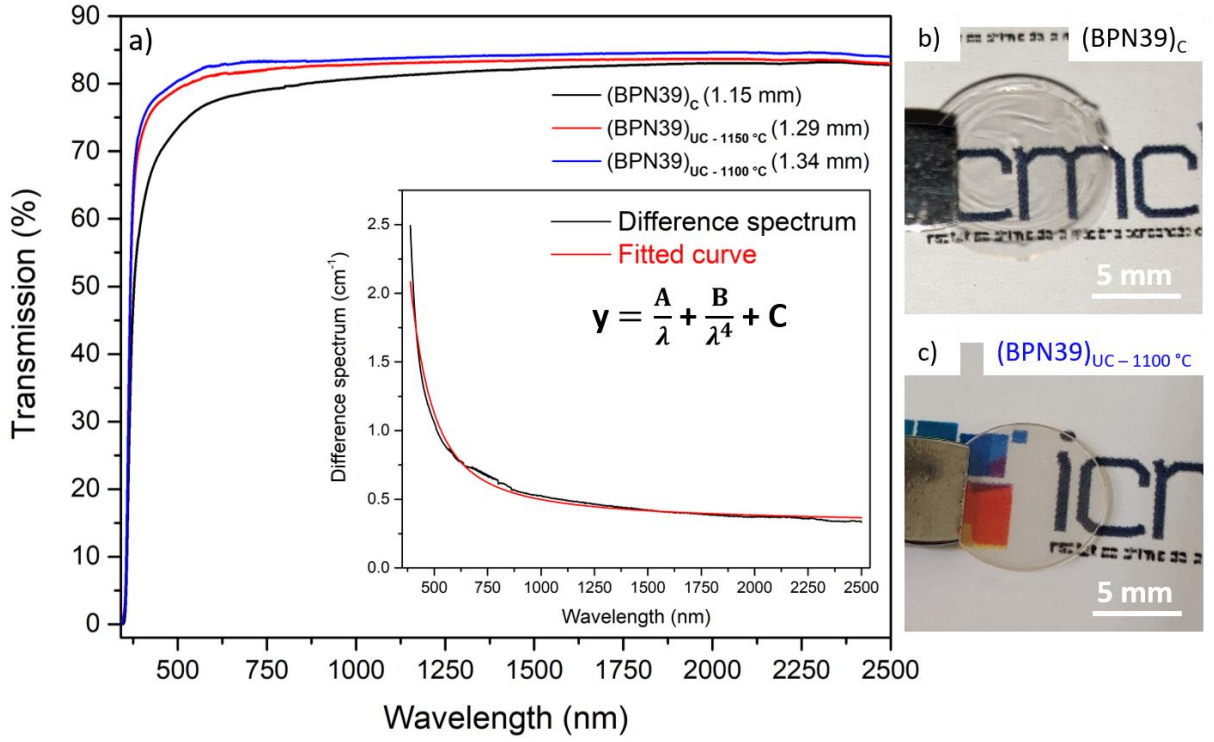

Fig 3. a) Optical transmission on BPN39 bulk polished samples synthesized by different methods :$(BPN39)_C$: casted; $(BPN39)_{UC\text{-}1150\,°C}$: uncasted at 1150 °C; $(BPN39)_{UC\text{-}1100\,°C}$: uncasted at 1100 °C. (inset: Absorption coefficient difference spectrum of the $(BPN39)_C$ and $(BPN39)_{UC\text{-}1100\,°C}$ samples and a fitted scattering curve as a function of the wavelength) b) Micrograph of the sample $(BPN39)_C$ and c) of the sample $(BPN39)_{UC\text{-}1100\,°C}$

The improvement of the optical quality and homogeneity of the glass can be visualized with the naked eye on the bulk polished samples (Figure 3.b, 3.c). Raman spectra performed on different spots of the casted sample could not highlight any structural variations, which indicates that the observed inhomogeneity relates purely to density variations frozen within the glass during quenching and not to chemical variations (Fig 2.a-SI). This result is in good agreement with the EDS image (Fig 2.b-SI) showing no remarkable contrast of the chemical composition in the areas the most rich in striae.

Multiple studies reported that the intensity of the scattered light in glasses is proportional to the magnitude of the density fluctuations [19-21]. Tsujikawa *et al.* [21] synthesized samples having different density fluctuations by using different fabrication treatment. They have recorded a decrease in the Rayleigh scattering coefficient in the samples having less density fluctuations than others of the same composition in pure, P_2O_5-doped and GeO_2-doped silica glasses.

The $(BPN39)_{UC\text{-}1100\,°C}$ glass exhibits very high transmission with almost no diffusion and an intrinsic absorption up to 350 nm due to the band gap absorption of niobium. This glass is used as a reference. The difference of the absorption coefficient spectrum between the $(BPN39)_C$ and $(BPN39)_{UC\text{-}1100\,°C}$ samples is shown in the inset of Figure 3.a. The intrinsic absorption of the two samples are the same. The difference is then mainly due to diffusion properties due to refractive index inhomogeneity as the density fluctuations leads to a local refractive index change in the material. The diffusion is assumed to be the combination of two main phenomena responsible for losses in optical glasses: Rayleigh scattering (< wavelength) and the diffusion linked to macrometric scales density fluctuations (Mie diffusion) of the sample. Figure 3.a shows the excellent fit as a function of the wavelength using (1) where A is the scattering coefficient for large object of the material, B the one due to Rayleigh scattering and C is a constant. If we consider that the spatial distribution of the refractive index in the

casted sample is assimilated to spherical particles of small size having different index than the surrounding glass, then the Rayleigh scattering coefficient can be described by the Rayleigh-Gans model as expressed in (2) [22] and an estimated size of the particles can be calculated. *N* is the particles number density, *V* the particles volume, *r* the particles radius, *n* the refractive index of the particles and Δ*n* is the index difference between the particles and the surrounding glass.

$$y = \frac{A}{\lambda} + \frac{B}{\lambda^4} + C \qquad (1)$$

$$B = \frac{2}{3} N V (2\pi)^4 r^3 (n.\Delta n)^2 \qquad (2)$$

In order to estimate the particles size in the $(BPN39)_C$ sample we consider $n((BPN39)_C) = 1.822$ as the index of the particles (Table 2). In addition n = 1.836 is the refractive index measured on the $(BPN39)_{UC\text{-}1100\,°C}$ sample, that gives us $\Delta n = n((BPN39)_{UC\text{-}1100\,°C}) - n((BPN39)_C) = 0.014$. From the fitting calculations, the particle radius is estimated to be 42 nm. One can say that the difference between the spectra is mostly inversely proportional to the fourth power of the wavelength as the relative weight of the factor B is 99% in front of A and C. This is a characteristic of optical attenuation caused by Rayleigh scattering. Despite the dominance of the term related to Rayleigh scattering one can not ignore the effect of the other two terms on the fitting equation as no proper fit can be obtained by removing one or both of them.

Angeli et al. [23] studied the influence of the temperature and quenching rate on the homogeneity of a borosilicate glass. They claimed that the quenching rate has a high impact on the homogeneity of the sample, slow rates being the more prone to preserve the homogeneity of the material. As well, *Levelut et al. [24]* studied the density fluctuations in silica glasses as a function of temperature and thermal history. They have assumed that those fluctuations are frozen in the glass at the fictive temperature, which is determined, by the cooling rate and the thermal history of the glass sample. The fictive temperature being the temperature at which the liquid structure is frozen into the glassy state where no further structural relaxation will occur. Moreover, it has been reported that density fluctuations and the scattering intensity are proportional to the fictive temperature of the glass [25, 26]. Therefore, the mitigation of these inhomogeneities are expected to lead to a remarkable improvement in the optical transparency of the sample. By cooling slowly, we can assume that the fictive temperature of the $(BPN39)_{UC\text{-}1100\,°C}$ sample is lower than that of the $(BPN39)_C$ sample. Thus, the remarkable differences on the overall homogeneity seen on the bulk samples between the two fabrication methods is mainly linked to the cooling rate of the glass and their resulting fictive temperature.

The spatial homogeneity of the refractive index is an important property that quantifies the quality of an optical glass. A glass with 10^{-4} and lower variation of the refractive index is considered as glass of optical quality [27]. In order to illustrate the inhomogeneity and defects in the samples due to refractive index variations, we visualize the samples using shadowscopy imaging. The shadowscopy is a direct projection technique that involves placing a transparent object to be studied between a light source and a screen receiving the light, with the objective to highlight light fluctuations on the screen due to refractive index variations within the material (Figure 4). Three samples having the same thickness (1 mm) were analyzed: a commercial microscope glass slide from Fischer, a casted BPN39 sample : $(BPN39)_c$ and an uncasted BPN39 one : $(BPN39)_{UC\text{-}1100\,°C}$. The raw images (Figure 4. b, c, d) captured on the camera were then processed and analyzed with various numerical spatial frequency filters on an equal selected zone for the different samples. First, a Gaussian filter F_G with a very low spatial cutoff frequency was applied for each raw image to remove high spatial frequency noise. This step enables us to have a reference image $[F_G(Im)]$ for each sample that makes it possible to overcome prismatic/lensing effects related to the topology or the shape of the polished sample. Secondly, on the same raw images, a convolution bandpass function F_Π apodized with a Gaussian function was applied

successively in the following interval [fmin; fmax = nyquist spatial frequency] (~45 steps) to obtain a replica of filtered image at different frequency [$F_\Pi(Im)$]. For each value of the spatial frequency, an estimated error was calculated with respect to the reference image of the sample (equation 3). N is the number of the pixels.

$$E = \frac{1}{N^2} \iint \frac{F_\Pi(Im) - F_G(Im)}{F_G(Im)} \quad (3)$$

The determination of the size of the defects and an estimation of the analyzed surface is obtained from the shadow analysis. Images observed on the screen correspond to a 2 mm diameter spot on the sample.

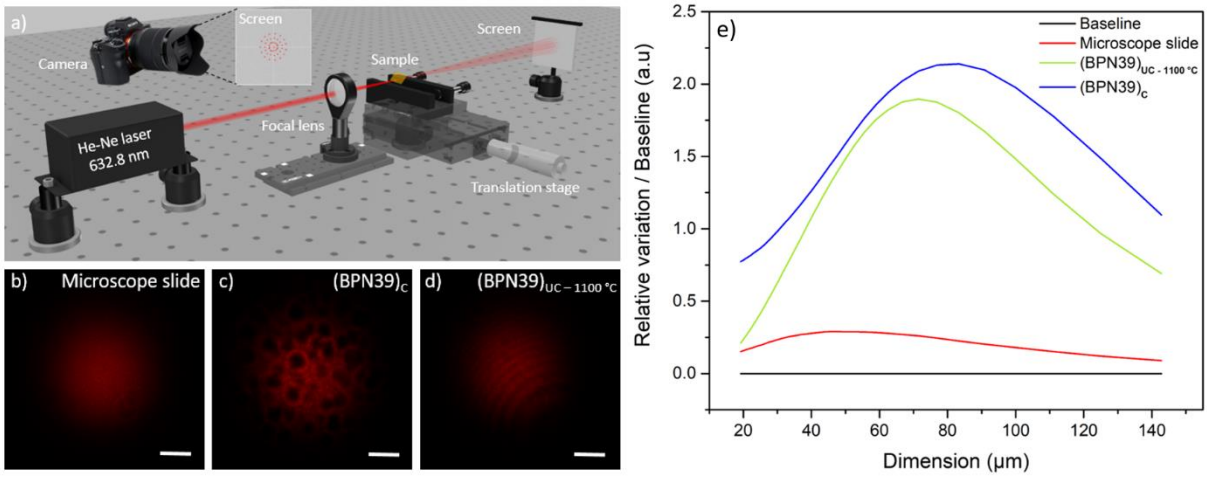

Fig 4. Shadowscopy imaging: a) Set-up of the experiment b) Micrograph of a Fischer microscope glass slide c) Micrograph of a casted sample $(BPN39)_c$ d) Micrograph of an uncasted sample $(BPN39)_{UC\text{-}1100\,°C}$ (scale bar = 2 cm) e) Relative variation of the striae magnitude as a function of their size

As shown in Figure 4.b, one can clearly see that the raw image of the microscope slide is very homogeneous. The appearing streaks are due to the interferences of the light waves passing through the sample since it could be slightly tilted on the sample holder. Unlike the microscope glass slide, the illumination contrast of the casted BPN39 sample projected on the screen exhibits variations between darker and brighter areas which have to be related to local frozen-in gradients of the refractive index (Figure 4.c). The darker area represent the striae in the sample. Note also that the image of the casted sample is larger than that of the other two since it is proportional to the amount of deflection caused due to the refractive index variations. The variation of the refractive index distorts the wave coming out of the sample, and the higher the spatial inhomogeneity of the refractive index is the wider the light rays will intercept the screen. In comparison, the imaging of the uncasted-1100°C sample exhibits a better homogeneity (Figure 4.d). Importantly, even though the samples are rotated with respect to the incident beam to discriminate between surface flaws and internal striae, some streaks remain visible due to the sample having faces not perfectly parallel. The raw images shows that the uncasted niobium borophosphate glass form homogeneous glasses with density fluctuations comparable to that of commercial microscope glass slide.

Furthermore, through image processing we calculate the variation of the magnitude of the striae of the different samples. The derivative of the error spectra calculated using equation 3 for each sample gives us the magnitude of the striae in the sample. This magnitude is compared as a function of the striae dimensions / spatial frequency for each sample with the baseline image, which is the image of the laser beam (Figure 4.e). As the image of the baseline is taken with no sample in the optical axis of the laser beam it is logical that the relative variation is equal to 0. The microscope slide with a very

good optical quality have a relative variation with a maximum at 0.28. Figure 4.e clearly evidences the difference between the commercial microscope slide and the synthesized glasses, as the latters have a relative variation around 2, approximatively eight times than that of the commercial glass. The uncasted sample $(BPN39)_{UC\text{-}1100\ °C}$ leads to a lower relative variations in the magnitude of striae compared to the casted sample $(BPN39)_C$ no matter their size. Lower striae magnitude means an improved homogeneity and a better optical quality. The shift of the maximum of the uncasted sample to the lower dimensions means that not only the magnitude of the striae is reduced but also their size. The striae of larger dimensions are mostly reduced by this technique since the relative variations compared to the baseline displays the largest increase at dimensions above 70 µm. It is important to note that all samples undergoes the same stirring protocol during the melting step prior to quenching, as it has been demonstrated that stirring affects positively the size of the striae and so the homogeneity of the glass [28]. This can be another way to reduce even further the size and magnitude of the striae in order to approach the optical quality of the commercial glass slide (red curve).

Shadowscopy gives qualitative insights on the optical quality of the glass sample, and how it relates to the quenching protocol applied to the melt. Following, casted and uncasted preforms were prepared and drawn into fibers. Attenuation measurements were measured by the cutback method at 1 µm on initial samples of ~2 meters in length (Figure 5). The fiber drawn from the uncasted preform shows an attenuation level ~3.19 dB/m, which is to say nearly as half as of the one drawn from a casted preform (~6.04 dB/m). It is worth noticing that this significant amelioration in attenuation is reached even though the casted preforms have a better polished surface than the uncasted ones who were mechanically drilled to obtain cylindrical preforms.

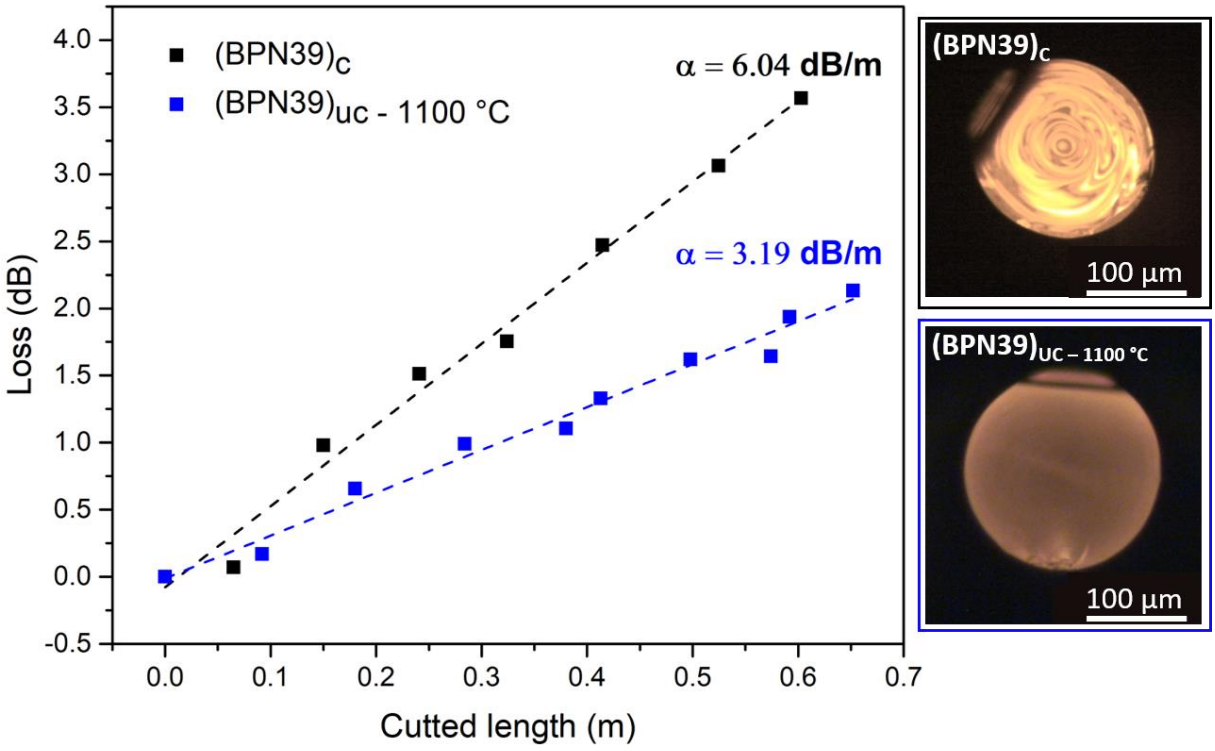

Fig 5. Optical attenuation at 1 µm on BPN39 fibers drawn from a casted preform (black) and from an uncasted preform (blue) along with the optical micrographs in transmission of the cross-section of the corresponding fibers.

One believes that the higher loss originates from the density fluctuations in the casted preform as clearly shown on the micrographs of the cross-section of the fibers. The density fluctuations lead to

local refractive index fluctuations generating light scattering and so higher optical attenuation. Although losses for the uncasted fiber remains relatively high for practical use, one must note that they were measured on mono-index fibers and that no purification protocol other than the use of high-purity precursors was introduced at this stage.

From the transmission measurements and the shadowscopy results, one can conclude to the occurrence of both a microscopic (~42 nm) and a macroscopic (~80-140 µm) altered refractive index variations in the material. One believes that our process improves both of them. Since the optical transmission and shadowscopy measurements were done on bulk samples but the optical loss on fibers, it is difficult to define which order of index variations our process improves the most. The cutback measurements show an improvement of the optical attenuation by nearly 50% between the two methods. Shadowscopy results shows a decrease of the striae magnitude by 20% for particles above 90 µm between the casted and uncasted sample, that is to say 40% of the decrease in the optical attenuation of the fibers. Assuming that the drawing process transfer in an homothetic manner the shape of the striae in the sample, and that the overlap factor between the guiding region and the region of the fiber containing the striae is equal to 1, one can say that the improvement in Rayleigh scattering due to density fluctuations leads to improving by 60% the optical attenuation in the BPN fibers. This improvement is partially due to the thermal history of the glass and its cooling rate. Cooling slowly decrease the fictive temperature in the glass which is proportional to the scattering coefficient due to density fluctuations [25]. As a result, one confirmed that the reduction in density fluctuations in niobium-rich borophosphate glass preforms reduces their optical attenuation nearly by half in the resulting glass fiber.

Refining of the elaboration method are in progress to reduce even further the probability of generating manufacturing related inhomogeneity into the preforms. In addition, one expects that direct improvements to fiber loss will be reached by improving the purity of the constituent materials and by producing polymer-coated core-clad fibers with core and clad compositions having appropriated amount of Nb_2O_5 to properly adjust their refractive indexes (Table 2). It is worth to mention that all preforms were drawn in the same temperature conditions in order to compare only the effect of the fabrication process on the optical losses. Drawing slowly at a lower temperature is considered to reduce even further the attenuation in optical fibers as demonstrated by Tsujikawa *et al.* on a GeO_2 doped silica fiber [25]. Finally, it is expected that tailoring of the $NaPO_3$ – $Na_2B_4O_7$ – Nb_2O_5 glass composition might represents a practical option to further reduce the magnitude of the density fluctuations. For instance Laberge *et al.* [29] showed such improvement could be reached by adding calcium oxide or alumina to binary Li_2O-SiO_2 glasses. Nonetheless, this path must be cautiously followed as one wants to preserve the optical properties of the material, namely its extended transmission in the near-IR as well as its high nonlinearity.

4 Conclusion

Explored here was the manufacturing of niobium-rich borophosphate glasses into fibers of optical quality. One shows that the glass with 39% Nb_2O_5 represents the upper limit for fiber drawing under oxygen. The relationship between glass processing and optical loss was investigated in order to guarantee the potential use of niobium borophosphate glasses as fiber optic waveguides. The smooth in-the-crucible quenching process mitigates density fluctuations within the glass matrix due to reduced temperature gradients and convection flows. As a result, fibers with significantly lower loss were produced. These results provide both insights into the interplay between chemical, rheological and optical properties of the near-infrared niobium borophosphate glasses as well as practical steps benefiting their shaping into glass optical fibers.

Acknowledgements

This work was supported by Agence Nationale de la Recherche (ANR) (ANR Grant ''TRAFIC'' N°62243) and by the Région Nouvelle-Aquitaine (Grant "F2MH" N°66245).

References

[1] T. Cardinal, E. Fargin, G. L. Flem, and S. Leboiteux, "Correlations between structural properties of Nb_2O_5-$NaPO_3$-$Na_2B_40_7$ glasses and non-linear optical activities," *Journal of Non-Crystalline Solids,* vol. 222, pp. 228-234, 1997.

[2] E. Fargin, A. Berthereau, T. Cardinal, J. J. videau, and A. Villeusuzzanne, "Contribution of theoretical chemistry to the investigation of optical non linearities in glasses," *Annales de Chimie Science des Matériaux,* vol. 23, pp. 27-32, 1998.

[3] T. Cardinal *et al.*, "Non linear optical properties of some niobium (V) oxide glasses," *Journal of Solid State Inorganic Chemistry,* vol. 33, pp. 597-605, 1996.

[4] M. Dussauze, E. Fargin, M. Lahaye, V. Rodriguez, and F. Adamietz, "Large second-harmonic generation of thermally poled sodium borophosphate glasses," *Optics Express,* vol. 13, pp. 4064-4069, 2005.

[5] M. Dussauze *et al.*, "Thermal poling of optical glasses: mechanisms and second-order optical properties," *International Journal of Appied Glass Science,* vol. 3, pp. 309-320, 2012.

[6] L. Karam *et al.*, "Electrically Micro-Polarized Amorphous Sodo-Niobate Film Competing with Crystalline Lithium Niobate Second-Order Optical Response," *Advanced optical materials,* vol. 8, no. 13, 2020.

[7] L. Petit *et al.*, "Fabrication and characterization of new Er^{3+} doped niobium borophosphate glass fiber," *Materials Science and Engineering,* vol. 117, pp. 283-286, 2005.

[8] N. L. Laberge, P. K. Gupta, V. Vasilescu, and P. B. Macedo, "Scattering losses in binary borate glasses," *Journal of Non-Crystalline Solids,* vol. 13, pp. 164-172, 1973.

[9] J. Schroeder, R. Mohr, P. B. Macedo, and C. J. Montrose, "Rayleigh and Brillouin scattering in K_2O-SiO_2 glasses," *Journal of the american ceramic society,* vol. 56, pp. 510-514, 1973.

[10] B. Zakharin and J. Stricker, "Schlieren systems with coherent illumination for quantitative measurements," *Applied optics,* vol. 43, pp. 4786 - 4795, 2004.

[11] G. S. Settles, *Schlieren and shadowgraph techniques*. Springer, 2001.

[12] J. Stroud, "Striae quality grades for optical glass," *Optical Engineering,* vol. 42, no. 6, pp. 1618-1624, 2003.

[13] S. Gaylord, B. Tincher, L. Petit, and K. Richardson, "Viscosity properties of sodium borophosphate glasses," *Materials Research Bulletin,* vol. 44, pp. 1031-1035, 2008.

[14] H. Smogor *et al.*, "Effect of silver on phase separation and crystallization of niobium oxide containing glasses," *Journal of Solid State Chemistry,* vol. 182, pp. 1351-1358, 2009.

[15] A. Zhang, A. Lin, and J. Toulouse, "Ultra-dry oxygen atmosphere to protect tellurite glass fiber from surface crystallization," *Journal of Non-Crystalline Solids,* vol. 356, pp. 525-528, 2010.

[16] M. R. Shahriari, T. Iqbal, and G. H. Sigel, "The effect of atmosphere on the surface crystallization of AlF_3 based glasses during fiber drawing," *Materials Science Forum,* vol. 67-68, pp. 263-270, 1991.

[17] A. Malakho, M. Dussauze, E. Fargin, B. Lazoryak, V. Rodriguez, and F. Adamietz, "Crystallization and second harmonic generation in thermally poled niobium borophosphate glasses," *Journal of Solid State Chemistry,* vol. 178, pp. 1888-1897, 2005.

[18] M. Dussauze, E. Fargin, A. Malakho, V. Rodriguez, T. Buffeteau, and F. Adamietz, "Correlation of large SHG responses with structural characterization in borophosphate niobium glasses," *Optical Materials,* vol. 28, pp. 1417-1422, 2005.

[19] N. L. Laberge, V. V. Vasilescu, C. J. Montrose, and P. B. Macedo, "Equilibrium Compressibilities and Density Fluctuations in K_2O-SiO_2 Glasses," *Journal of the american ceramic society,* vol. 56, pp. 506-509, 1973.

[20] C. Levelut *et al.*, "Density fluctuations in oxide glasses investigated by small-angle X-ray scattering," *Journal of Applied Crystallography,* vol. 40, pp. 512-516, 2007.
[21] K. Tsujikawa, K. Tajima, and J. Zhou, "Intrinsic loss of optical fibers," *Optical fiber technology,* vol. 11, pp. 319-331, 2005.
[22] A. Sakamoto, Y. Himei, and T. Seto, "Applicability of optical scattering model to β-Quartz solid solution glass-ceramics with nanoscalecrystalline phase," *Journal of the american ceramic society,* vol. 91, pp. 2570-2574, 2008.
[23] F. Angeli *et al.*, "Effect of temperature and thermal history on borosilicate glass structure," *Physical review,* vol. B 85, no. 5, p. 054110, 2012.
[24] C. Levelut, A. Faivre, R. L. Parc, B. Champagnon, J. L. Hazemann, and J. P. Simon, "In situ measurements of density fluctuations and compressibility in silica glasses as a function of temperature and thermal history," *The American Physical Society,* vol. 72, no. 22, p. 224201, 2005.
[25] K. Tsujikawa, K. Tajima, and M. Ohashi, "Rayleigh Scattering Reduction Method for Silica-Based Optical Fiber," *Joutnal of lightwave technology,* vol. 18, pp. 1528 - 1532, 2000.
[26] S. Sakaguchi and S.-i. Todoroki, "Rayleigh scattering of silica core optical fiber after heat treatment," *Applied optics,* vol. 37, pp. 7708-7711, 1998.
[27] P. Hartmann, "Optical glass: standards – present state and outlook," *Advanced Optical Technologies,* vol. 4, no. 5-6, pp. 377-388, 2015, doi: doi:10.1515/aot-2015-0047.
[28] M. Jensen and Y. Yue, "Effect of stirring on striae in glass melts," *Journal of Non-Crystalline Solids,* vol. 358, pp. 349-353, 2011.
[29] N. L. Laberge, P. K. Gupta, and P. B. Macedo, "Density fluctuations in silicate glasses," *journal of Non-Crystalline Solids,* vol. 17, pp. 61-70, 1974.

Supporting Information

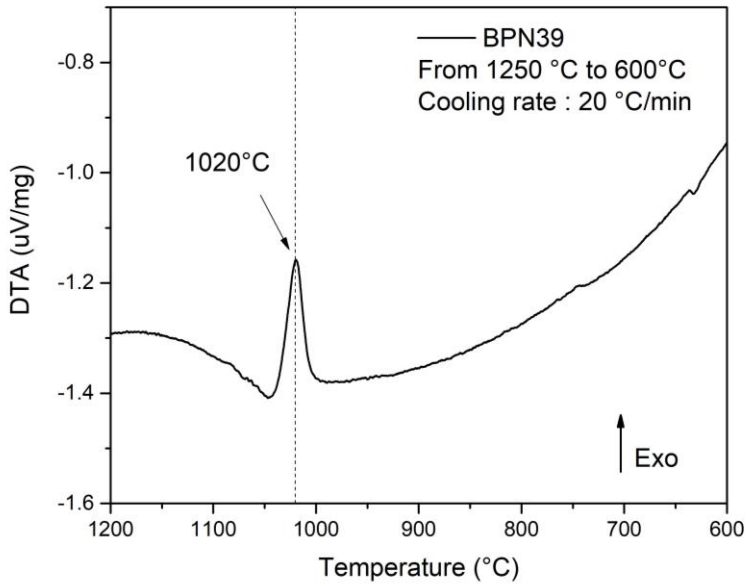

SI. 1 - The crystallization temperature while cooling the melt of BPN39 identified by DTA

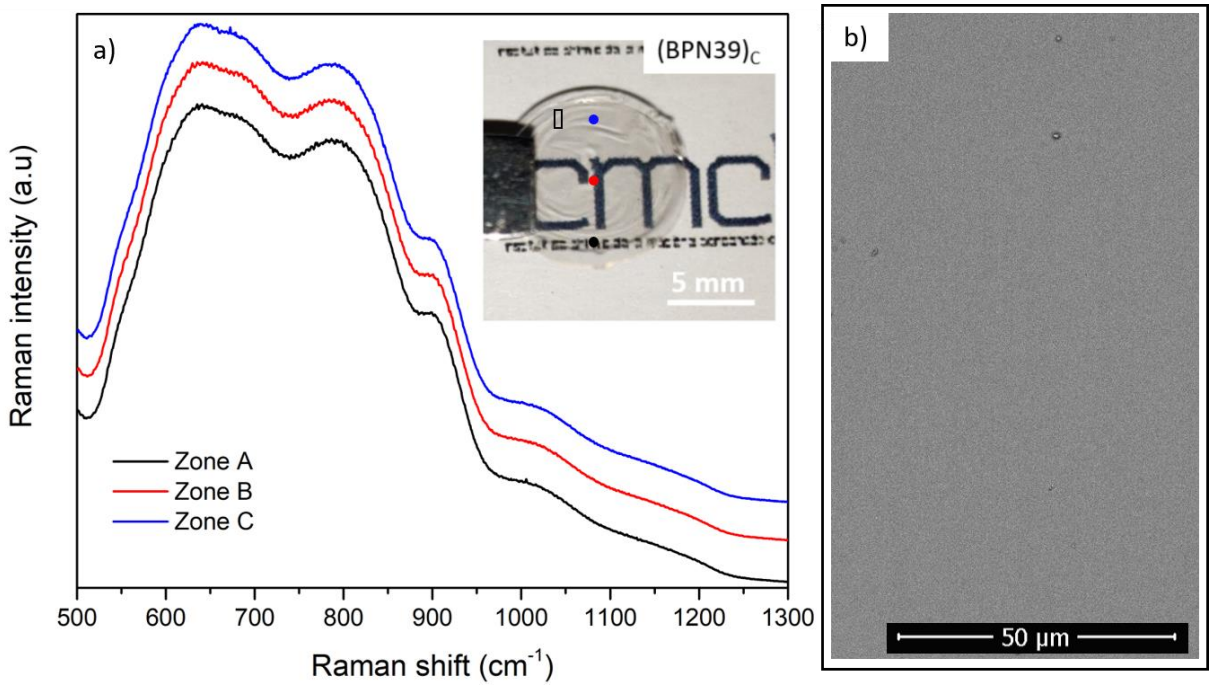

SI. 2 – a) Normalized Raman spectra on different zones of the $(BPN39)_C$ sample. b) EDS image on the striae area (black rectangular) of the $(BPN39)_C$ sample.